A simple design of ultra-broadband and polarization insensitive terahertz metamaterial absorber

Ben-Xin Wang · Ling-Ling Wang · Gui-Zhen Wang · Wei-Qing Huang · Xiao-Fei Li · Xiang Zhai

Abstract Ultra-broadband metamaterial absorbers have attracted considerable attention due to their great prospect for practical applications. These absorbers are usually stacked by many (no. <20) different shaped or sized sub-units in a unit cell, making it quite troublesome to be fabricated. Simple design for ultra-broadband absorber is urgently necessary. Herein, we propose a simple design of ultra-broadband and polarization insensitive terahertz metamaterial absorber based on a double-layered composite structure on a metallic board, and each layer consists of two sets of different sized square metallic plates. Greater than 90 % absorption is obtained across a frequency range of 0.85 THz with the central frequency around 1.60 THz. The relative absorption bandwidth of the device is greatly improved to 53.3 %, which is much larger than previous results. The mechanism of the ultra-broadband absorber is attributed to the overlapping of four closely resonance frequencies. The proposed metamaterial absorber has potential applications in detection, imaging and stealth technology.

1 Introduction

Recently, metamaterials, with the sub-wavelength scale unit cell, have attracted intense attention due to their exotic properties that are unavailable in nature, such as invisibility, superlensing and negative refraction. Split ring resonators (SRRs) [1, 2], fishnet structures [3], cut wire pairs [4] and other stereostructures [5] have been proposed for the landmark predictions of metamaterial theory. In most applications, the absorption loss of the metamaterials often degrades the performance. For artificial light absorber, however, the absorption loss becomes useful and can be significantly enhanced by proper design of the structure.

The first perfect metamaterial absorber composed of a metallic split ring and a cut wire separated by a dielectric layer was demonstrated by Landy et al. [6], and achieved a measured absorptivity of 88% at 11.48 GHz. From then on, metamaterial perfect absorbers have been extensively demonstrated in every relevant spectra range including microwaves [7–9], terahertz [10], infrared [11] and optical frequencies [12]. Although they have a high absorptivity, the above-mentioned perfect absorbers are single-band absorption, which greatly hampers their practical applications. Subsequently, some improvement works were followed to make the absorber operate at dual-band [13] and triple-band [14] absorptions. Unfortunately, these efforts have common shortcomings of narrow absorption bandwidth. In pragmatic applications, it is desirable to have perfect absorption over broader spectra bands.

By combining several narrowband resonant frequencies together and packing them closely by varying the geometric parameters of different component in a unit cell, broadband resonance metamaterials can be obtained. Following this design strategy, broadband metamaterial absorbers have been widely demonstrated from the microwave region to the optical region [7, 8, 15–21]. For example, Luo et al. [7] and Liu et al. [8] presented the broadband absorbers based on multiple square metallic plates in the microwave frequencies. Ye et al. [15] and Grant et al. [16] demonstrated wideband perfect absorbers by stacking multiple different sized metallic crosses in the

B.-X. Wang (✉) · L.-L. Wang · G.-Z. Wang · W.-Q. Huang · X.-F. Li · X. Zhai
School of physics and Microelectronic and Key Laboratory for Micro-Nano Physics and Technology of Hunan Province, Hunan University, Changsha 410082, China
e-mail: wangbenxin@hnu.edu.cn

terahertz region. Cheng et al. [17] and Hendrickson et al. [18] obtained broadband perfect absorbers by using multiplexed plasmonic metallic nanostructures in the infrared region. However, the absorption bandwidth, in particular greater than 90% absorption bandwidth is not wide enough. In many cases, ultra-broadband absorption is required, such as stealthy technology and solar energy harvesting.

Very recently, several significant advancements in designing the ultra-broadband absorbers by stacking multiple (no. <20) metal-dielectric layers were demonstrated by Cao et al. [22], Cui et al. [23] and Ding et al. [24]. These proposed absorbers possessed excellent absorption performance with W_{RAB} (relative absorption bandwidth, which is defined as $W_{RAB} = 2(f_u - f_l)/(f_u + f_l)$ [24], where f_u and f_l are the upper and lower limits of a frequency range with absorption above 90 %, respectively) >50 %. In the fabrication, however, it is quite difficult to exactly align the relative position of each patterned metallic structure, in particular at higher frequencies such as terahertz, infrared and visible regions. To design the ultra-broadband absorber, hence, it is urgently necessary to reduce the stacked layers as much as possible.

Herein, we demonstrate a simple design of ultra-broadband and polarization insensitive absorber formed by a double-layered composite structure on a metallic ground plane, and each layer consists of two sets of different sized square metallic plates. The W_{RAB} of the device is greatly improved to 53.3 %, which is much larger than previously reported values. The mechanism for the ultra-broadband absorption originates from the overlapping of four different but closely positioned resonance frequencies. Particularly, the resonance frequency of each absorption peak can be flexible, controlled by varying the size of the corresponding metallic plate and the proposed absorber is easier to be fabricated by electron-beam lithography (EBL) or focused ion-beam milling (FIB) than previous structures [15, 16, 22–25].

2 Structure and design

A unit cell of the compact metamaterial absorber structure is illustrated in Fig. 1a–c, which consists of two alternating layers of patterned metallic plates and dielectric layers, and a metallic board at the bottom (see Fig. 1a). Each layer consists of two sets of different sized square metallic plates (Fig. 1b, c represents the one- and two-layer of the patterned metallic array, respectively). The geometric parameters of the designed ultra-broadband metamaterial absorber are marked in Fig. 1. The repeat period is $P = Px = Py = 170$ μm, and the length of the square plates A, B, C and D is $l_1 = 45$ μm, $l_2 = 38$ μm, $l_4 = 60$ μm and $l_3 =$
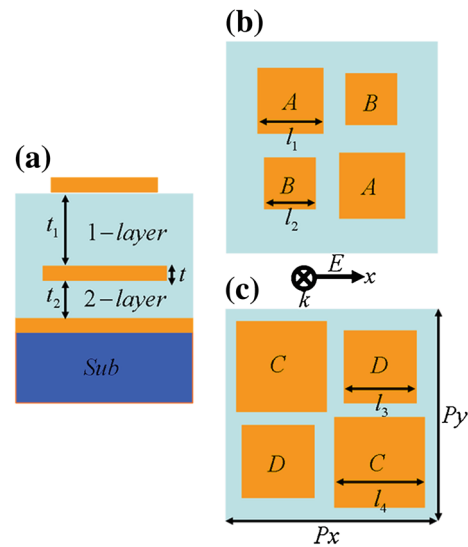

Fig. 1 Cross section (**a**) and top views of the metallic arrays of the designed one-layer (**b**) and two-layer (**c**) ultra-broadband absorber

50 μm. The square plates A and B, C and D are offset from each other by 43.5 and 30 μm in two lateral dimensions in the unit cell, respectively. The thicknesses of each dielectric slab (polyimide) are set to $t_1 = 11.3$ μm and $t_2 = 9.5$ μm, and then the thickness of the metal (Au) is $t = 0.4$ μm with a frequency independent conductivity of $\sigma = 4.09 \times 10^7$ Sm^{-1}. The dielectric constant of polyimide [13] in the frequency of interest is $\varepsilon = 2.4 + i0.005$. Our results are obtained through finite-difference time-domain (FDTD) simulations, where the periodic structures are illuminated by a normally incident plane wave with the electric field parallel to the x-axis. Perfectly matched layers (PML) are applied along the z direction and periodic boundary conditions in the x and y directions. The absorption coefficient, A is obtained by $A = 1 - T - R$, where T (transmission) is very close to zero as the thickness of the metallic board is much larger than its skin depth, and then the absorption is calculated by $A = 1 - R$. The absorption (A) may achieve perfect absorption when the R (reflection) is close to zero (i.e., impedance ($z = 1$) matched to the free space).

3 Simulation results and discussion

Figure 2a shows the calculated absorption spectra of the proposed ultra-broadband absorber. As shown in Fig. 2a, the absorption spectra consist of six resonance frequencies, located at the frequencies of 1.26 THz (f_1), 1.49 THz (f_2), 1.76 THz (f_3), 1.93 THz (f_4), 2.30 THz (f_5) and 2.67 THz (f_6) (with the absorption coefficients of 98.58, 98.14, 99.73, 99.96, 59.93 and 92.46 %), respectively. It is obvious that a

Fig. 2 **a** Absorption spectra of the designed ultra-broadband absorber; **b** absorption spectra of the designed absorber with different repeat period P
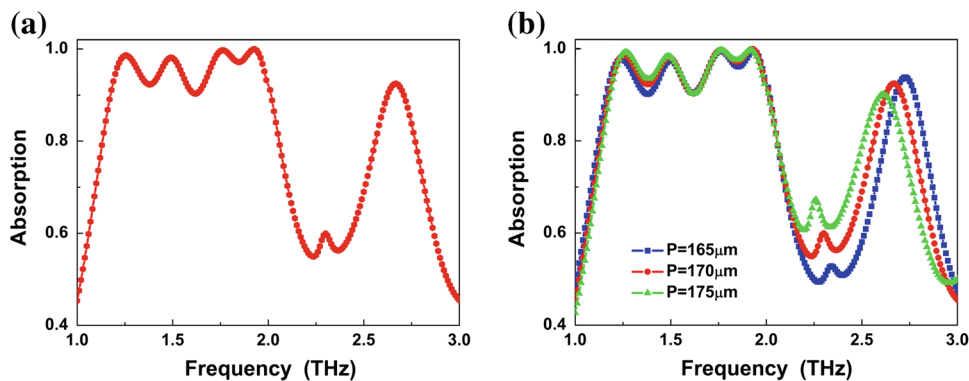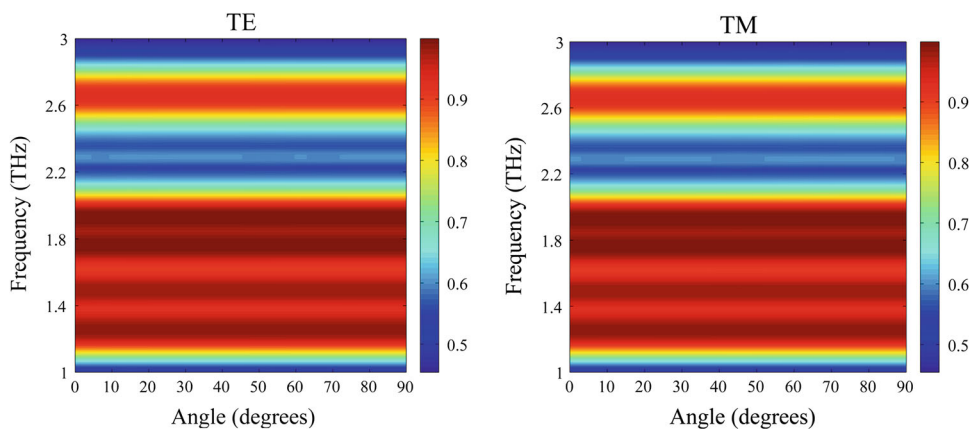

Fig. 3 Calculated absorption spectra under different polarization angles for TE and TM waves


large absorption bandwidth with the absorption coefficient >90 % is obtained over a frequency range of 0.85 THz (covers the 1.17–2.02 THz range) for the first four closely positioned resonances. The W_{RAB} of the device is equal to 53.3 %, which is much larger than those reported in references [7, 8, 18, 19]. Besides, owing to the high degree symmetric (fourfold symmetric structure) of the square metallic plates A, B, C and D, the designed ultra-broadband absorber is insensitive to the polarization of the incident electromagnetic wave (see below Fig. 3). Actually, the first four absorption peaks result from the strong magnetic resonance in different sized metallic–dielectric–metallic structures (see the distribution of the magnetic field in below Fig. 4a₁–a₄) which is just like the case of the single-layered absorber structure [6–8, 10–12], while the fifth and sixth absorption peaks arise from the interaction of neighboring unit cells or the sub-cells, i.e., the higher-order resonance absorption peaks. To give an intuitive evidence, Fig. 2b shows the calculated absorption spectra of the designed absorber under different period P. It is obvious that the frequencies f_5 and f_6 both shift to higher frequencies with the decrease of the period P [26–28], while the changes of the f_1, f_2, f_3 and f_4 are neglected. In general, the diffraction angle of the higher-order resonance absorption peak can be described by the grating equation [28]:

$$\sin\theta = \frac{\lambda_n}{np} \tag{1}$$

where λ_n and P are the frequency of the higher-order resonance absorption peak and the repeat period of the designed absorber, respectively, and n is an integer. The calculated first (f_5) and second (f_6) orders diffraction angle for $P = 170$ μm is about 50° and 41°, respectively. Obviously, the frequencies f_5 and f_6 are both inversely proportional to the repeat period P.

To better understand the physical origin of the proposed ultra-broadband absorber, we give the calculated magnetic ($|H_y|$) [the plane of y is equal to the center of the square plates A and B (along the x-axis) not the plane of the B and A (along the x-axis)] and electric fields ($|E|$) (Fig. 4b, c represents the center plane of the one- and two-layer patterned metallic plates, respectively) distributions corresponding to the four absorption maximums (f_1, f_2, f_3 and f_4) in Fig. 4. Different field distributions are observed for the frequencies at 1.26, 1.49, 1.76 and 1.93 THz. As shown in Fig. 4a₁, the distribution of the magnetic field in the mode f_1 is mainly focused on the bottom left dielectric layer of the absorber, while only a very small section of magnetic resonance can be observed in the other part of the dielectric layer. Great enhancement of the magnetic field in the dielectric layer indicates that the large charge accumulates
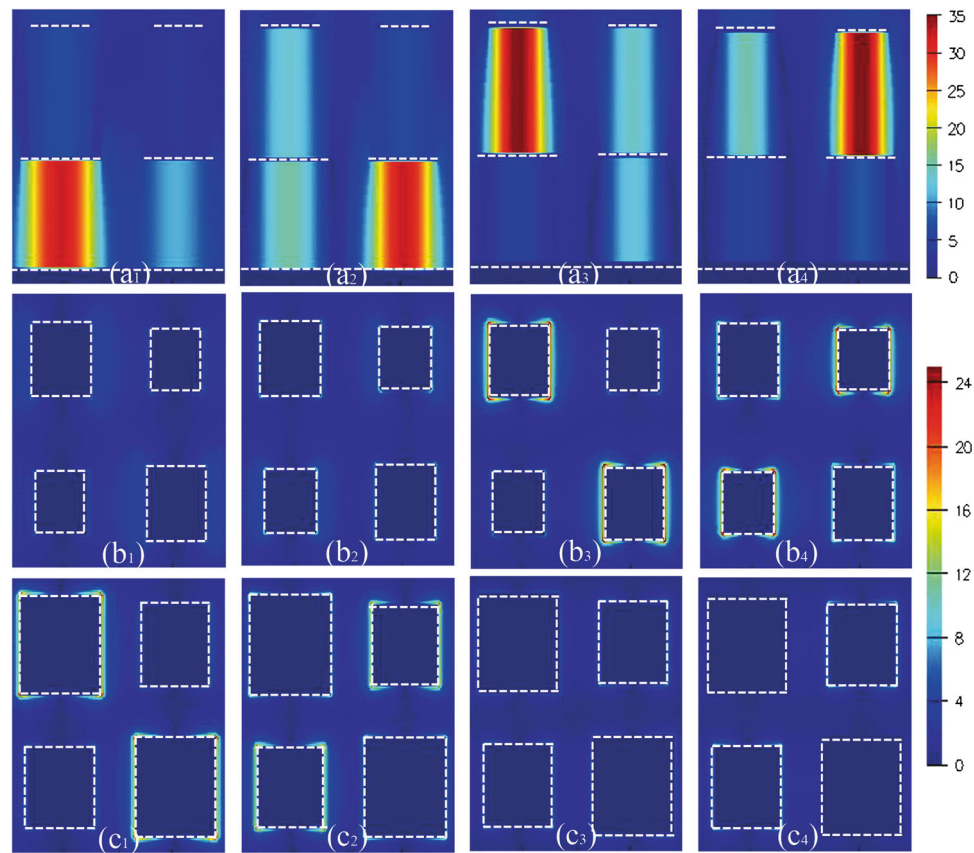
at the edges of the square patch. Thus, the distribution of the electric field is mainly focused on both sides of the metallic array (along the direction of the electric field) [7, 8, 18]. It is obvious that the electric field distribution of the mode f_1 is primarily gathered in the edges of the left and right sides of the top left and bottom right square plates (i.e., the longest metallic plate C) in the two-layer metallic array, while scarcely electric field distribution can be observed in the top right and bottom left square plates (D) in the same layer as well as the metallic square plates (A and B) array of the one-layer (see Fig. 4b$_1$, c$_1$). And for mode f_2, the distributions of magnetic and electric fields are mainly focused on the bottom right dielectric layer and both sides (left and right) of the top right and bottom left square plates (i.e., the metallic plate D) in the two-layer metallic array, respectively, while the distributions of the magnetic and electric fields are neglected in other parts of the dielectric layers or metallic plates array. Similarly, the magnetic distribution in the mode f_3 (or f_4) is mainly focused on the top left (or the top right) dielectric layer, and the corresponding the distribution of the electric field is mainly concentrated at the left and right sides of the top left and bottom right (or the top left and bottom right) square metallic plates in the one-layer metallic array. According to the LC circuit model, the frequency of the metamaterial is given by [15, 29]:

$$f = \frac{1}{2\pi\sqrt{LC/2}} \sim \frac{1}{l} \tag{2}$$

where l is the length of the square plate. From the Eq. 2, we can acknowledge that the frequency of the absorber is inversely proportional to the length of the square plate. As shown in Fig. 1b, c, the length of the square plates C, D, A and B decreases gradually, thus the frequencies f_1, f_2, f_3 and f_4 increase accordingly. Obviously, the combination of the first four absorption peaks determines the ultra-broadband absorption. Different from previous reports by combing several different sized resonators to obtain a resonance absorption peak [22–24], the frequency of each absorption peak arises from the corresponding individual square metallic plate. Therefore, the frequencies f_1, f_2, f_3 and f_4 can be flexible, controlled by independently re-shaping different metallic plates (see below Fig. 5). The proposed absorber has a wide application prospect in detection, stealth and solar cells and can be easily fabricated using electron-beam lithography (EBL) or focused ion-beam milling (FIB).

After the mechanism of the ultra-broadband absorption has been explained, the influence of some geometric parameters on the absorption can be easily understood. As discussed above, the frequency f_1 (or f_4) mainly depends on the length of the square plate B (l_2) [or C (l_4)]. Thus, with

Fig. 5 Dependence of the absorption spectra on the length l_4 (**a**) and l_2 (**b**) of the designed absorber

(a)

(b)
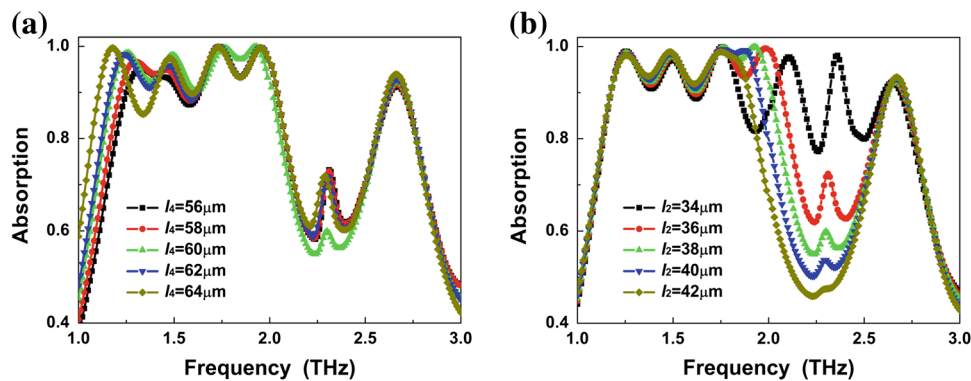
the other geometric parameters fixed, the change of the length of the square plate B (or C) can nearly determine the upper (or lower) limit of the absorption. Fig. 5a, b shows the influence of the size of the square plates C and B on the resonance frequencies and absorption coefficients, respectively. It is obvious that as the length of the square plate C is increased, f_L becomes small while f_U and other resonance absorption peaks are nearly fixed, which results in the increase of the W_{RAB} (see Fig. 5a). Similarly, for the change of the square plate B, the f_U gradually increases with the decrease of the length of the plate B, while the changes of the other absorption peaks (f_1, f_2 and f_3) are neglected (see Fig. 5b). Obviously, the change of the square metallic plate B (or C) provides the ability to broaden the absorption bandwidth. However, the changes of the square plates B and C cannot be too large because their supported resonance frequencies will vary too quickly and lead to some strong oscillation appearing on the absorption spectra (see the dark yellow curves in Fig. 5a, b). Actually, besides the changes of the upper and lower limits of the ultra-broadband absorption, the modes f_2 and f_3 are also easily controlled by varying the size of the corresponding patterned metallic plates D and A, respectively (not shown here).

4 Conclusion

In conclusion, we demonstrate a simple design of ultra-broadband and polarization insensitive terahertz metamaterial absorber formed by a double-layered composite structure on a metallic ground plane, and each layer consists of two sets of different sized square metallic plates. Greater than 90 % absorption is obtained over a frequency range of 0.85 THz. The relative absorption bandwidth of the device is greatly improved to 53.3 %, which is much larger than the previous results. The four patterned square metallic plates resonating at different but close frequencies result in the ultra-broadband absorption. An equivalent LC resonant circuit is proposed to analyze the origin of the

broadband performance. Moreover, the design gives a considerable freedom to shift or even broaden the absorption band by independently reshaping different metallic plates. A further broadening of the absorption bandwidth is possible by increasing the number of stacked layers, and the concept could be readily extended to other frequency regimes for a host of applications such as detection, imaging and solar cell.

References

1. J.B. Pendry, A.J. Holden, D.J. Robbins, W.J. Stewart, IEEE Trans. Microw. Theory Tech. **47**, 2075 (1999)
2. B.X. Wang, L.L. Wang, G.Z. Wang, L. Wang, X. Zhai, X.F. Li, W.Q. Huang, Opt. Commun. **303**, 13 (2013)
3. J. Yang, C. Sauvan, H.T. Liu, P. Lalanne, Phys. Rev. Lett. **107**, 043903 (2011)
4. G. Dolling, C. Enkrich, M. Wegener, J.F. Zhou, C.M. Soukoulis, S. Linden, Opt. Lett. **0**, 3198 (2005)
5. N. Liu, H. Liu, S. Zhu, H. Giessen, Nat. Photon **3**, 157 (2009)
6. N.I. Landy, S. Sajuyigbe, J.J. Mock, D.R. Smith, W.J. Padilla, Phys. Rev. Lett. **100**, 207402 (2008)
7. H. Luo, Y.Z. Cheng, R.Z. Gong, Eur. Phys. J. B **81**, 387 (2011)
8. Y.H. Liu, S. Gu, C.R. Luo, X.P. Zhao, Appl. Phys. A **108**, 19 (2012)
9. A. Dimitriadis, N. Kantartzis, T. Tsiboukis, Appl. Phys. A **109**, 1065 (2012)
10. H. Tao, C.M. Bingham, A.C. Strikwerda, D. Pilon, D. Shrekenhamer, N.I. Landy, K. Fan, X. Zhang, W.J. Padilla, R.D. Averitt, Phys. Rev. B **78**, 241103 (2008)
11. J.A. Mason, G. Allen, V.A. Podolskiy, D. Wasserman, IEEE Photon. Tech. Lett. **24**, 31 (2012)
12. C. Hu, Z. Zhao, X. Chen, X. Luo, Opt. Express **17**, 11039 (2009)
13. Y. Ma, Q. Chen, J. Grant, S.C. Saha, A. Khalid, D.R.S. Cumming, Opt. Lett. **36**, 945 (2011)
14. X. Shen, T.J. Cui, J. Zhao, H.F. Ma, W.X. Jiang, H. Li, Opt. Express **9**, 9401 (2011)
15. Y. Ye, Y. Jin, S. He, J. Opt. Soc. Am. B **27** , 498 (2010)
16. J. Grant, Y. Ma, S. Saha, A. Khalid, D.R.S. Cumming, Opt. Lett. **36**, 3476 (2011)

17. C.W. Cheng, M.N. Abbas, C.W. Chiu, K.T. Lai, M.H. Shih, Y.C. Chang, Opt. Express **20**, 10376 (2012)
18. J. Hendrickson, J. Guo, B. Zhang, W. Buchwald, R. Soref, Opt. Lett. **37**, 371 (2012)
19. Y. Cui, J. Xu, K.H. Fung, Y. Jin, A. Kumar, S. He, N.X. Fang, Appl. Phys. Lett. **99**, 253101 (2011)
20. L. Huang, D.R. Chowdhury, S. Ramani, M.T. Reiten, S.N. Luo, A.J. Taylor, H.T. Chen, Opt. Lett. **37**, 154 (2012)
21. Y. Cheng, Y. Nie, R. Gong, Opt. Laser Technol. **48**, 415 (2013)
22. S. Cao, W. Yu, T. Wang, Z. Xu, C. Wang, Y. Fu, Y. Liu, Appl. Phys. Lett. **102**, 161109 (2013)
23. Y. Cui, K.H. Fung, J. Xu, H. Ma, Y. Jin, S. He, N.X. Fang, Nano Lett. **12**, 1443 (2012)
24. F. Ding, Y. Cui, X. Ge, F. Zhang, Y. Jin, S. He, Appl. Phys. Lett. **100**, 103506 (2012)
25. Q. Liang, T. Wang, Z. Lu, Q. Sun, Y. Fu, W. Yu, Adv. Opt. Matter. **1**, 43 (2013)
26. L. Li, Y. Yang, C. Liang, J. Appl. Phys. **110**, 063702 (2011)
27. W.J. Padilla, A.J. Taylor, C. Highstrete, M. Lee, R.D. Averitt, Phys. Rev. Lett. **96**, 107401 (2006)
28. M. Pu, M. Wang, C. Hu, C. Huang, Z. Zhao, Y. Wang, X. Luo, Opt. Express **20**, 25513 (2012)
29. J. Zhou, E.N. Economon, T. Koschny, C.M. Soukoulis, Opt. Lett. **31**, 3620 (2006)